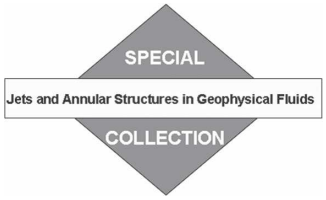

Multiple Jets as PV Staircases: The Phillips Effect and the Resilience of Eddy-Transport Barriers

D. G. DRITSCHEL

Mathematical Institute, University of St. Andrews, St. Andrews, United Kingdom

M. E. MCINTYRE

Centre for Atmospheric Science, Department of Applied Mathematics and Theoretical Physics, University of Cambridge, Cambridge, United Kingdom

(Manuscript received 29 June 2006, in final form 23 March 2007)

ABSTRACT

A review is given that focuses on why the sideways mixing of potential vorticity (PV) across its background gradient tends to be inhomogeneous, arguably a reason why persistent jets are commonplace in planetary atmospheres and oceans, and why such jets tend to sharpen themselves when disturbed. PV mixing often produces a sideways layering or banding of the PV distribution and therefore a corresponding number of jets, as dictated by PV inversion. There is a positive feedback in which mixing weakens the "Rossby wave elasticity" associated with the sideways PV gradients, facilitating further mixing. A partial analogy is drawn with the Phillips effect, the spontaneous layering of a stably stratified fluid, in which vertically *homogeneous* stirring produces vertically *inhomogeneous* mixing of the background buoyancy gradient. The Phillips effect has been extensively studied and has been clearly demonstrated in laboratory experiments. However, the "eddy-transport barriers" and sharp jets characteristic of extreme PV inhomogeneity, associated with strong PV mixing and strong sideways layering into Jupiter-like "PV staircases," with sharp PV contrasts $\Delta q_{\rm barrier}$, say, involve two additional factors besides the Rossby wave elasticity concentrated at the barriers. The first is shear straining by the colocated eastward jets. PV inversion implies that the jets are an essential, not an incidental, part of the barrier structure. The shear straining increases the barriers' resilience and amplifies the positive feedback. The second is the role of the accompanying radiation-stress field, which mediates the angular-momentum changes associated with PV mixing and points to a new paradigm for Jupiter, in which the radiation stress is excited not by baroclinic instability but by internal convective eddies nudging the Taylor–Proudman roots of the jets.

Some examples of the shear-straining effects for strongly nonlinear disturbances are presented, helping to explain the observed resilience of eddy-transport barriers in the Jovian and terrestrial atmospheres. The main focus is on the important case where the nonlinear disturbances are vortices with core sizes $\sim L_D$, the Rossby (deformation) length. Then a nonlinear shear-straining mechanism that seems significant for barrier resilience is the shear-induced disruption of vortex pairs. A sufficiently strong vortex pair, with PV anomalies $\pm\Delta q_{\rm vortex}$, such that $\Delta q_{\rm vortex} \gg \Delta q_{\rm barrier}$, can of course punch through the barrier. There is a threshold for substantial penetration through the barrier, related to thresholds for vortex merging. Substantial penetration requires $\Delta q_{\rm vortex} \gtrsim \Delta q_{\rm barrier}$, with an accuracy or fuzziness of order 10% when core size $\sim L_D$, in a shallow-water quasigeostrophic model. It is speculated that, radiation stress permitting, the barrier-penetration threshold regulates jet spacing in a staircase situation. For instance, if a staircase is already established by stirring and if the stirring is increased to produce $\Delta q_{\rm vortex}$ values well above threshold, then the staircase steps will be widened (for given background PV gradient β) until the barriers hold firm again, with $\Delta q_{\rm barrier}$ increased to match the new threshold. With the strongest-vortex core size $\sim L_D$ this argument predicts a jet spacing $2b = \Delta q_{\rm barrier}/\beta \sim L_{\rm Rh}^2\,(U_{\rm vortex})/L_D$ in order of magnitude, where $L_{\rm Rh}(U_{\rm vortex}) = (U_{\rm vortex}/\beta)^{1/2}$, the Rhines scale based on the peak vortex velocity $U_{\rm vortex}$, when $2b \gtrsim L_{\rm D}$. The resulting jet speeds $U_{\rm jet}$ are of the same order as $U_{\rm vortex}$; thus also $2b \sim L_{\rm Rh}^2(U_{\rm jet})/L_D$. Weakly inhomogeneous turbulence theory is inapplicable here because there is no scale separation between jets and vortices, both having scales $\sim L_D$ in this situation.

Corresponding author address: Michael E. McIntyre, Department of Applied Mathematics and Theoretical Physics, Wilberforce Rd., Cambridge CB3 0WA, United Kingdom.
E-mail: mem@damtp.cam.ac.uk

DOI: 10.1175/2007JAS2227.1

1. Introduction

Chaotic flows in stratified, rotating fluid systems like planetary atmospheres and oceans are often called "turbulent." However, in such systems there is no such thing as turbulence without waves, a point well brought out in the celebrated paper of Rhines (1975). One way to appreciate the point is to note that such systems always have background gradients of potential vorticity (PV) and then consider the implications for the momentum and angular momentum budgets. As will be illustrated here, those budgets make no sense at all, in realistic cases, unless one considers the wavelike and turbulent aspects together.

As well as short-range turbulent momentum transports of the *austausch* or mixing-length kind, there are long-range momentum transports due to Rossby waves and other wave types—"radiation stresses" in the language of physics. Indeed, the ubiquity and importance of such stresses illustrates one of the grand themes of physics, the "dynamical organization of fluctuations" with systematic mean effects (also important in, e.g., biological molecular motors). By its very nature, a wave propagation mechanism such as the Rossby wave mechanism will *organize* the fluctuating fields, no matter how chaotic they may seem, in the sense of inducing systematic correlations among them. The correlations are shaped by the waves' polarization relations and usually give rise to long-range stresses. They may produce phenomena like planetary equatorial superrotation, or gyroscopically pumped global-scale circulations such as the Brewer–Dobson circulation of the terrestrial stratosphere.[1] The range of such stresses is not limited to mixing lengths, but can reach out as far as waves can propagate. And, crucially, there is a strong dynamical interplay between the more wavelike and the more turbulent aspects, not unlike the wave–turbulence interplay and stress divergence that give rise to alongshore currents in an ocean beach surf zone.

Among the consequences of such interplay, in stratified, rotating systems, are three interrelated phenomena on which this review will focus: first the spatial inhomogeneity of PV mixing by layerwise-two-dimensional turbulence, second the common occurrence of "antifrictional" or upgradient horizontal stresses $\overline{u'v'}$, and third the spontaneous creation and self-sharpening, or narrowing, of jets.

The three phenomena are all illustrated by the typical jet-sharpening scenario sketched in Fig. 1. The sketch was originally made to help understand the behavior of the terrestrial winter stratospheric polar-night jet, or polar-vortex edge, during a so-called minor warming. However, with appropriate rescaling it applies equally well to other cases such as that of the subtropical tropopause jet in the late stages of a nonlinear baroclinic wave life cycle of type 1 (LC1; e.g., Thorncroft et al. 1993). In both cases the PV is strongly mixed on the equatorward flank of the jet (Fig. 1a), reshaping the large-scale PV distribution and causing the velocity profile to sharpen, in the sense that its lateral scale becomes narrower (Fig. 1b), with concomitant changes in the angular momentum distribution. Fundamentally similar jet-sharpening processes have often been observed in laboratory and numerical experiments, with PV mixing on one or both flanks of the jet, going back to the pioneering work of Fultz et al. (1959), Hide (1958), and N. A. Phillips (1956).[2] More recent work clearly showing jet sharpening in its simplest, barotropic form includes, for instance, the beautiful laboratory experiments of Sommeria et al. (1989, 1991), and many numerical experiments on the related phenomenon of vortex erosion or stripping (e.g., Juckes and McIntyre 1987; Legras et al. 2001). The reader may gain entry to the most recent literature from, to pick a very few, Vallis and Maltrud (1993), Rhines (1994), Nozawa and Yoden (1997), Hughes (1996), Manfroi and Young (1999), Huang et al. (2001), Robinson (2006), McWilliams (2006, his chapter 5), Greenslade and Haynes (2008), Scott and Polvani (2007), Sukoriansky et al. (2007), and Thompson and Young (2007),

[1] Quantitative illustrations of the radiation stresses in action, evaluated in the standard way as so-called Eliassen–Palm fluxes [Eq. (A.2) below] may be found for mechanistic models and for the real stratosphere in, for instance, Dunkerton et al. (1981), Rosenlof (1995), and in very many other publications. The gyroscopic pumping mechanism is well understood and was thoroughly analyzed in Haynes et al. (1991). Ekman pumping is a special case. [Websearch "gyroscopic pumping of the Brewer–Dobson circulation" for a recent tutorial including online animations.] The vertical component of the Eliassen–Palm flux is what oceanographers call the "form drag" or, more aptly, the "form stress," across undulating stratification surfaces (Bretherton 1969). It arises from correlations between pressure fluctuations and surface slopes and typifies the dynamical organization of fluctuations. Strictly speaking one should include not only *radiation* but also *diffraction* stresses, for instance driving the summer branch of the Brewer–Dobson circulation, or mediating the Eady baroclinic instability viewed as a pair of counterpropagating, and vertically diffracting, Rossby waves (Lighthill 1963, p. 93; Bretherton 1966b; Hoskins et al. 1985; Methven et al. 2005).

[2] Norman A. Phillips, a great pioneer in atmospheric dynamics and numerical weather prediction, then working at Princeton with primitive computer technology, is not to be confused with Owen M. Phillips of the "Phillips effect," a great pioneer in ocean waves and turbulence then working at Cambridge, United Kingdom.

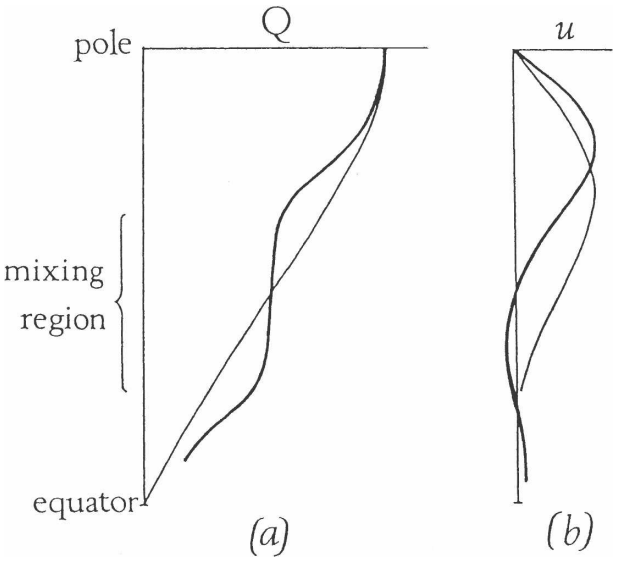

FIG. 1. Schematic from McIntyre (1982), suggesting the robustness of nonlinear jet sharpening by inhomogeneous PV mixing. Here most of the mixing is on the equatorward flank of an idealized stratospheric polar-night jet, in a broad midlatitude "surf zone" due to the breaking of Rossby waves arriving from below. The profiles can be thought of as giving a somewhat blurred, zonally averaged picture. The light and heavy curves are for conditions before and after the mixing event, where "after" means "after the wave has largely decayed." The difference between the two zonal velocity curves on the right is dictated by inversion of the difference between the two PV curves on the left, like smoothed versions of Eq. (5.1) and Fig. 7b since over several scale heights the middle stratosphere behaves qualitatively like a shallow-water model with L_D roughly on the order of 2000 km (Robinson 1988; Norton 1994). Vortex stretching associated with the horizontally narrowing jet scale increases the relative vorticity at the Pole (e.g., Dunkerton et al. 1981, Figs. 4, 5). Angular momentum is reduced even though the jet is sharpened. Long-range radiation stresses cannot be neglected. For Jovian and terrestrial ocean jets, with their relatively smaller latitudinal scales, the mixing is typically strong on both sides of each jet (e.g., Marcus 1993; Hughes 1996). In the Jovian case the mixing is almost certainly due to a different stirring mechanism altogether, namely, convection in the planet's interior (see footnote 4 and section 8).

as well as from the other papers in this special collection.

The jet-sharpening and angular-momentum changes are tied to the PV mixing via PV inversion (e.g., Hoskins et al. 1985; Robinson 1988). Specific illustrations will be given in Eqs. (5.1)–(7.2) below. PV inversion is usually robust for jets. Invertibility depends only on the jets behaving as balanced flows. The imbalance represented by inertia–gravity and sound waves is negligible in many cases, or unimportant after averaging (e.g., Viúdez and Dritschel 2004). It follows that the link between PV mixing and jet sharpening is very tight. During mixing, if it occurs, the stress pattern has no choice but to fit in with the angular momentum changes dictated by inversion. Conversely, if there is no way to set up a suitable stress pattern, then PV mixing may be modified or inhibited.

In quasigeostrophic models, with the Rossby wave mechanism as the only available wave mechanism, the way the stress pattern fits in is described by the well-known *Taylor identity* relating stress divergences to eddy PV fluxes, recalled in the appendix. The stresses themselves extend between regions of PV mixing and, in general, outside them as well. As already noted, in principle they can extend as far as waves can propagate. The stress pattern associated with the example in Fig. 1 (e.g., Edmon et al. 1980; Dunkerton et al. 1981) corresponds mainly to Rossby waves propagating or diffracting up the jet axis from below with their characteristic upward–westward phase tilt, then refracting equatorward and breaking in the mixing region indicated in Fig. 1a. That region can therefore be thought of as a "Rossby wave surf zone." A characteristic feature of the stress pattern is the well-known antifrictional westward–equatorward tilt of phase lines between the jet and the adjacent surf zone, signaling positive values of $\overline{u'v'}$. As is well known, the existence and statistical persistence of this feature used to be regarded as a major enigma of atmospheric science (e.g., Lorenz 1967, 149–151; Starr 1968).

Figure 1, then, can be taken as a reminder of the main concepts needed to solve that enigma, indeed to solve it in a remarkably robust and simple way. They are (i) the PV invertibility principle and its corollaries (which include making sense of the Rossby wave mechanism itself), (ii) the fact that breaking Rossby waves mix PV (though usually imperfectly), and (iii) the Taylor identity, Eq. (A.3) below, helping to show how the whole wave–turbulence jigsaw fits together.

Historically—perhaps because concept (i) was not put together with scenarios like Fig. 1a—the solution emerged only rather tortuously, over the second half of the past century, in several parallel strands of research that gradually broke away from the competing turbulence-theoretic austausch paradigms of the first half called "momentum transfer theory" and "vorticity transfer theory." Jeffreys, early in the century, was the first to establish from the angular momentum principle that an antifrictional stress $\overline{u'v'}$ is required to explain the surface westerlies (Jeffreys 1926). The actual existence of a stress with the right sign and magnitude was confirmed midcentury, from the newly available upper-tropospheric data, by Starr and others. Lewis (1998) gives an excellent review. The first credible modeling effort—a fully nonlinear baroclinic instability simulation exhibiting antifrictional $\overline{u'v'}$ and jet sharpening

within a simplified but dynamically consistent framework, two-layer quasigeostrophy—was reported in the landmark paper of Phillips (1956). That paper, along with an increasingly clear recognition that neither of the old austausch paradigms would work (Eady 1950, 1954), stimulated renewed efforts toward mechanistic understanding.

There was first a long line of linear baroclinic instability studies showing that the fastest-growing modes on broad jets usually exhibit antifrictional $\overline{u'v'}$ (e.g., Eady 1954; Eliasen 1961; Pedlosky 1964; Eady as reported in Green 1970; Stone 1969; McIntyre 1970; Simmons 1974; Held 1975; Juckes 2000; Methven et al. 2005). Held's paper broke new ground by using the Taylor identity, in its three-dimensional form (A.3) first published by Bretherton (1966a), to demonstrate explicitly the robustness, within linear theory, of the $\overline{u'v'}$ pattern with phase lines tilting in what was sometimes called the "obvious" way, as if advected by the horizontal shear, even though "not really obvious without the analysis, since the instability mode involves a subtle balance between advection and propagation effects" (McIntyre 1970, p. 285). Second, and still within linear theory, PV invertibility was used to crystallize our understanding of the Rossby wave mechanism and its role in baroclinic instability viewed as counterpropagating Rossby waves (Bretherton 1966b; see also, e.g., Hoskins et al. 1985; Lighthill 1963, p. 93; Methven et al. 2005). Third, recognition dawned that Rossby wave radiation from nonlinear midlatitude disturbances would be likely to produce the required $\overline{u'v'}$ pattern in a robust and statistically stable way.

In hindsight (e.g., Edmon et al. 1980; Thorncroft et al. 1993; Hughes 1996) we can now recognize this third idea as the most important of the three, as a contribution to mechanistic understanding of the simplest, most robust, and most basic kind. It appears from Green (1970) that the idea first occurred to Eady, though it seems that Dickinson (1969) arrived at it independently while working in Starr's group at the Massachusetts Institute of Technology and was the first to publish it. Then at Woods Hole Thompson (1971) proposed it again, it seems, independently, and Whitehead (1975) demonstrated Rossby wave-induced $\overline{u'v'}$ patterns and momentum changes in an elegant and highly influential, laboratory experiment. Dickinson's paper was remarkable for the way in which, despite using nothing but the apparatus of linear Rossby wave theory, it not only postulated the nonlinear wave generation now familiar from the baroclinic life cycle studies and first made conspicuous in the paper by Edmon et al. (1980), but also pointed implicitly toward the final wave-breaking stage. Rather than in a broad surf zone, the latter was hidden inside an infinitesimal "critical line singularity" in Dickinson's analysis, a linear-theoretic artifact whose real significance is that linear theory is predicting its own breakdown. The implied wave–turbulence interplay, involving antifrictional $\overline{u'v'}$ fields, was later verified and illuminated by the discovery of idealized but fully consistent models of *nonlinear* Rossby wave critical layers (Stewartson 1978; Warn and Warn 1978; Killworth and McIntyre 1985; Haynes 1989). Such "layers" are finite, though narrow, surf zones. Those models provided mechanistically clear and explicit illustrations of the precise way in which PV mixing can influence the wave-induced $\overline{u'v'}$ field and angular momentum budget well outside the mixing region, and the precise way in which the Taylor identity is satisfied.

Complementing all this was yet another parallel strand of history starting with the theoretical work of Rhines (1977). It used weakly inhomogeneous turbulence theory, assuming a scale separation between large-scale mean fields and small-scale turbulent eddies and Rossby waves, to build a model of the wave–turbulence interplay within that limitation but again recognizing the insight furnished by the Taylor identity. The scale separation facilitated the inclusion of cases with nontrivial zonal as well as meridional structure.

A typical feature of PV mixing scenarios like that of Fig. 1 is, however, the strong inhomogeneity of the mixing, which precludes scale separation (e.g., McIntyre and Palmer 1983; Juckes and McIntyre 1987; Riese et al. 2002). Today's remote sensing techniques have made this inhomogeneity more conspicuous than ever, in the case of the real terrestrial winter stratosphere, by showing in remarkable detail many examples of breaking Rossby waves with both their turbulent and their wavelike aspects visible in sharply contrasted adjacent regions. One typically sees the wavelike edge of the polar vortex with its steep isentropic gradients of PV colocated with the polar-night jet axis, immediately adjacent to the surrounding surf zone, reminding us that Fig. 1 gives only a blurred view of reality.[3] And PV-mixing scenarios of just this kind have become increas-

[3] For the "remarkable detail" in today's sharper view of reality, websearch "gyroscopic pump in action" to see a movie of remote sensing data from the work of Riese et al. (2002). Notice not only the sharpness of the polar vortex edge but also the remarkable completeness of the sideways mixing, in the surf zone on the equatorward flank of the polar-night jet, as revealed by a nearly passive chemical tracer, nitrous oxide. Tracers do not, of course, behave in parallel with PV in all circumstances, but in this example the PV distribution is almost certainly very similar. See also, for instance, Waugh et al. (1994).

ingly familiar from high-resolution chemical–dynamical modeling motivated by the stratospheric ozone problem (e.g., within a vast literature; Manney et al. 1994; Simmons et al. 2005; and the review by Haynes 2005).

In the next section of this review we argue that the extreme inhomogeneity is itself a generic consequence of the wave–turbulence interplay, in some circumstances at least. Thus we widen the scope to include not only classic cases like Fig. 1 but also cases like Jupiter, in which a stratified layer is stirred in what is almost certainly a different way, namely by buoyant convection[4] and associated radiation stresses. The central idea is simply that of *positive feedback,* an unstable competition between wavelike and turbulent dynamics. It leads us to expect, for instance, the spontaneous emergence of quasi-permanent jets when an initially homogeneous system is stirred homogeneously.

Part of the feedback is due simply to the nature of the Rossby wave restoring mechanism, which depends on background PV gradients. To that extent it is like the "Phillips effect" (O. M. Phillips 1972), the spontaneously inhomogeneous vertical mixing of the background buoyancy gradient in a stably stratified fluid. However, in section 2 we argue as in Juckes and McIntyre (1987) that jet *shear,* producing shear straining of vortical disturbances, can greatly enhance the feedback. The arguments are tested against some nonlinear numerical experiments in sections 3 and 4. The experiments provide further mechanistic insight not only into the terrestrial but also, arguably, into aspects of the Jovian case.

Despite the different stirring mechanism or mechanisms, the Jovian case is like that of the terrestrial winter stratosphere to the extent that the PV-mixing inhomogeneity appears to be at an extreme, with staircase-like PV profiles of many steps in the Jovian case as compared with a single step in the terrestrial case. Strong arguments for a Jovian staircase have been made by Marcus (1993), from the observed vortex-interaction phenomenology. Sections 5 and 6 discuss the implied scaling laws for step width, that is, for jet spacing. Section 7 briefly reviews the way PV inversion dictates angular-momentum changes, also pointing out that channel and doubly periodic beta-plane models may have artificial constraints on their angular momentum that conceal those changes. Section 8 offers a few concluding remarks including a new suggestion about Jupiter. For completeness the Taylor identity is reviewed in a brief appendix.

2. The Phillips effect for buoyancy and PV, and the formation of eddy-transport barriers

The Phillips effect for vertical buoyancy mixing was clearly demonstrated in the classic experiment of Ruddick et al. (1989), in which stirring by an array of vertical rods, setting no vertical scale, produced layering in a stratified tank. See also, within an extensive literature, the original discussion by O. M. Phillips (1972) and the elegant mathematical modeling studies by Barenblatt et al. (1993) and Balmforth et al. (1998). Those studies were, however, limited by vertical austausch or local flux-gradient assumptions. In a more general way, not dependent on austausch assumptions, one may argue heuristically that the observed layering results simply from a positive feedback process. The background buoyancy gradient and gravity wave elasticity are weakened in a mixing layer, facilitating further mixing across stratification surfaces. Conversely, the gravity wave elasticity is strengthened wherever interfaces are forming between the mixed layers, inhibiting mixing across the interfaces.

In the case of the quasi-horizontal, lateral mixing of PV *along* stratification surfaces, one can make a similar positive-feedback argument in terms of the Rossby-wave restoring mechanism, that is, the quasi-elasticity of sideways undulating PV contours. The background gradient and Rossby elasticity are weakened in a mixing region, facilitating further mixing, and conversely are strengthened wherever PV contours are bunched together between mixed regions (e.g., McIntyre 1994, p. 308). Thus, other things being equal, large-scale PV gradients are liable to be weakened in some regions and sharpened in others, making them more turbulent and more wavelike respectively. The extreme, staircase-like instances of this include the terrestrial stratosphere

[4] The visible layer of vortical motion on Jupiter, marked by ammonia cirrus clouds, is stably stratified and is presumed to overlie deeper layers in which thermocompositional convection transports the heat flux known to emanate from the planet's interior, ending up in plumes a bit like terrestrial cumulonimbus clouds (e.g., Rogers 1995; Ingersoll et al. 2004, section 6.5). Solar heating has a somewhat comparable magnitude, but would be unlikely by itself to build a significant pole-to-equator temperature gradient, because of the "convective thermostat" effect (e.g., Ingersoll 1976a,b; Stone 1976; Ingersoll and Porco 1978; Rogers 1995, p. 275). A pole-to-equator temperature gradient such as that assumed in Williams (2003) to support baroclinic instability would seem unlikely to be sustainable. To have a continuous distribution of potential temperature with such a gradient, while avoiding gross static instability, there would have to be an underlying stably stratified layer with its strongest stratification at the equator (Allison 2000, Fig. 2; Williams 2003, Fig. 6). Such a layer would tend to inhibit internal convection in such a way as to reduce the pole-to-equator temperature gradient. That is presumably why hardly any such gradient is observed in reality, in the upper layers most strongly affected by solar radiation.

where the wavelike regions of sharpened gradients have been clearly shown, through a wealth of chemical data, to be able to shut off the mixing almost completely. That is, the wavelike regions with their associated eastward jets act as "eddy-transport barriers" (e.g., Juckes and McIntyre 1987; Nakamura 1996; Haynes and Shuckburgh 2000; Marshall et al. 2006; Haynes et al. 2007). Other such examples include the laboratory experiments of Sommeria et al. (1989, 1991)—confirming the barrier and staircase structure both by dye injection and by PV measurements using velocimetry—and the classic demonstration by Danielsen (1968) of a sharp barrier at a tropopause-jet axis, strikingly revealed by airborne observations of nuclear test debris. Marcus (1993) argues persuasively for barriers and staircases on Jupiter from model experiments showing generically realistic vortex-interaction behavior. In particular, the experiments show the eastward jets acting as barriers against vortex excursions. All these would appear to be extreme cases of the positive feedback or PV Phillips effect in action.

However, Rossby elasticity is by no means the same thing as the static stability or buoyancy elasticity acting in the Ruddick et al. experiment. Furthermore, there is no counterpart of PV inversion in the buoyancy case. That is, buoyancy layering does not necessarily cause jet formation and indeed does not, in fact, cause it in the Ruddick et al. (1989) experiments. And, as noted by Juckes and McIntyre (1987), in the PV case jet shear can act to enhance the barrier effect, hence the positive feedback effect, in an important way. In their words—referring to an early high-resolution model of stratospheric Rossby wave breaking, jet sharpening, and barrier formation in a scenario like that of Fig. 1—the Rossby elasticity "works most effectively on the largest spatial scales." This is connected with the way Rossby elasticity depends on PV inversion, which, in contrast with the buoyancy case, is a nonlocal functional relation. Thus Rossby elasticity "cannot explain the remarkable imperviousness of the main vortex even to small-scale incursions." That "remarkable imperviousness," a clear-cut case of the barrier effect, is also, they go on to say, "related ... to the existence of strong horizontal shear."

At small enough scales, differential advection by the shear overwhelms Rossby wave elasticity in the well-known way (e.g., Yamagata 1976), leading to the passive-tracer-like behavior of weak small-scale PV anomalies, conspicuous in the form of the filamentation seen in Juckes and McIntyre's model and in many other high-resolution numerical experiments including, most strikingly, experiments at infinite Reynolds number using accurate contour advection without "surgery" (e.g., Dritschel 1989). Such behavior is no more than would be expected from the standard Kelvin–Orr theory of "sheared disturbances" or "shear straining" (Thomson 1887; Orr 1907; Yamagata 1976). But the Rossby wave and Kelvin–Orr theories are both *linear*, as is the more recent "shear-sheltering" theory of Hunt and Durbin (1999).

For all those theories can tell us, real nonlinear surf-zone turbulence might make the vortex edge, for instance, not barrier-like but sieve-like in the sense of allowing the free exchange of material between the vortex interior and exterior on scales too small to feel Rossby elasticity. In any case, the effectiveness or otherwise of eddy transport barriers is clearly a fundamental problem in dynamics as well as chemistry and, in particular, intimately part of the whole question of why the positive feedback seems so effective, why jets are ubiquitous, and why, for instance, Jovian vortices behave as they do. To our knowledge, there has never been a case of a real Jovian vortex crossing an eastward jet (Rogers 1995; Rogers 2006, personal communication). In the next section, therefore, we revisit the eddy-transport-barrier problem in a way that focuses on its nonlinear aspects.

3. Barrier-penetration experiments

In this section we illustrate by simple numerical experiments at near-infinite Reynolds number how the barrier effect is crucially enhanced by the shear on the flank of a jet, even in a highly nonlinear disturbance regime. The standard quasigeostrophic shallow-water model is used, with Lagrangian contour-dynamics methods in a polar tangent plane approximation, with the winter stratosphere in mind. We focus on realistic values 1000–2000 km of the Rossby length L_D, as judged by nonlinear shallow-water behavior that best mimics the real stratosphere (Norton 1994). Thus we avoid rigidly bounded models, that is, nondivergent barotropic dynamics, $L_D = \infty$. Rigid upper boundaries are of course unrealistic for atmospheres. And, though realistic for some aspects of ocean dynamics, models with $L_D = \infty$ are not closely relevant to oceanic layerwise-two-dimensional turbulence with bottom topography, influenced as it is much more by baroclinic L_D values.

The model is defined by

$$Dq/Dt = 0 \tag{3.1}$$

where $q = f + \mathcal{L}(\psi)$, the quasigeostrophic PV, with constant Coriolis parameter f and with $\mathcal{L}(\psi) = (\nabla^2 - L_D^{-2})\psi$. The domain is horizontally unbounded, so that the PV inversion to find the streamfunction ψ is

$$\psi = \mathcal{L}^{-1}(q - f) = -\frac{1}{2\pi}\int\int K_0\left(\frac{|\mathbf{x} - \mathbf{x}'|}{L_D}\right)[q(\mathbf{x}') - f]d^2\mathbf{x}', \tag{3.2}$$

where $K_0(\cdot)$ is the modified Bessel function decaying exponentially for large argument. The two-dimensional velocity field is $(u, v) = (-\partial\psi/\partial y, \partial\psi/\partial x)$, so that the material derivative $D/Dt = \partial/\partial t + u\partial/\partial x + v\partial/\partial y$, to leading order.

We take an idealized version of the winter stratosphere with a perfectly developed "staircase step," that is, with a sharp-edged polar vortex. For simplicity it is taken to be a large vortex patch of uniform PV, surrounded by an idealized surf zone of infinite extent having a smaller uniform PV value. This corresponds to an exaggerated version of the heavy curves in Fig. 1, with a discontinuous jump in PV on the left and a slope discontinuity in zonal velocity on the right, like one of the sharply peaked jets in Fig. 7 below. We take L_D = 2000 km and polar-vortex radius 3000 km in the examples shown. Values L_D = 1000 km and L_D = 1500 km were also used, giving qualitatively similar results. The PV contrast between the polar vortex and surf zone is denoted by $\Delta q_{\text{barrier}}$. We have found that straightening out the vortex edge, making it into a channel-model jet with the same PV contrast, makes little difference to the behavior.

We test the resilience of the barrier at the vortex edge by bombarding it with the most powerful of coherent vortex structures, namely fast-propagating vortex pairs. A sufficiently strong vortex pair will punch through any given barrier, and a sufficiently weak one will not. Many experiments were done with vortex pairs of various strengths and sizes, incident from various directions. In all cases where the incident vortex pair gets anywhere near the barrier—which requires the vortex pair to be sent in an upshear direction—the resulting behavior can reasonably be called shear-induced disruption of the vortex pair, a kind of "divide and rule." The experiment shown in Fig. 2 illustrates this behavior.

The polar vortex is central in the top left panel. A large, tightly spaced, fast-propagating vortex pair is incident upshear at 225°. Its members have relative strengths $\Delta q_{\text{vortex}}/\Delta q_{\text{barrier}} = \pm 1.0$; thus the strength of the cyclonic member matches that of the barrier. This is a strongly nonlinear situation in which the entire polar vortex is violently disturbed. Nevertheless, the shear outside the barrier quickly separates the two members of the vortex pair, disrupting its ability to propagate. Consequently—even though the barrier suffers a very large Rossby wave distortion, comparable to that in a minor stratospheric warming—only modest amounts of vortex-pair and other surf-zone material penetrate well inside. Figure 3 enlarges the ninth and twelfth panels of Fig. 2 to show the detail more clearly. The grayscaling distinguishes material from, in order from lightest to darkest, the ambient surf zone, the incident anticyclone, the incident cyclone, and the polar vortex.

The shear-induced disruption of the incident vortex pair involves more than just pulling it apart. The anticyclonic member survives intact, staying well outside the barrier and corotating with the ambient shear in the manner familiar from classic vortex-interaction studies (e.g., Kida 1981; Bell 1990). By contrast, most of the material of the cyclonic member of the pair is sheared out into a long filament, and most of the filament gets wrapped round the edge of the polar vortex, itself cyclonic. Some of the cyclonic material is promptly ejected back into the surf zone, in a familiar and typical kind of Rossby wave-breaking or barrier-erosion event (e.g., Juckes and McIntyre 1987; Polvani and Plumb 1992). That event is seen in the bottom row of Fig. 2. Of the remaining incident-cyclone material, some of it stays near the polar-vortex edge, though a modest amount ends up deeper inside.

If we make the size of the incident vortex pair smaller, keeping its relative strength at ± 1.0, then it propagates more slowly, is disrupted sooner, and penetrates less. The same occurs if the relative strength is reduced below 1.0. Even for large, fast vortex pairs like that of Fig. 2, the barrier is very resilient against deep penetration for relative strengths $\lesssim 0.9$. By contrast, for relative strengths $\gtrsim 1.1$, substantial amounts of material from the incident cyclone (though never from the anticyclone in the cases considered) penetrate deeply into the polar vortex. Figure 4 shows the most violent case considered, like that of Figs. 2–3 except that the incident vortex pair has relative strength ± 1.4. Then a large portion of the incident cyclone penetrates all the way into the polar vortex. The incident anticyclone again remains isolated. Similar results were obtained for L_D = 1000 km and L_D = 1500 km.

For practical purposes it seems accurate enough to summarize all these cases by saying, for incident vortex-core sizes within a modest numerical factor of L_D, that the transition from very little penetration to substantial penetration corresponds to

$$\left|\frac{\Delta q_{\text{vortex}}}{\Delta q_{\text{barrier}}}\right| \sim 1.0 \pm 0.1. \tag{3.3}$$

For core sizes more substantially different from L_D, the thresholds are somewhat higher. Also, we have found

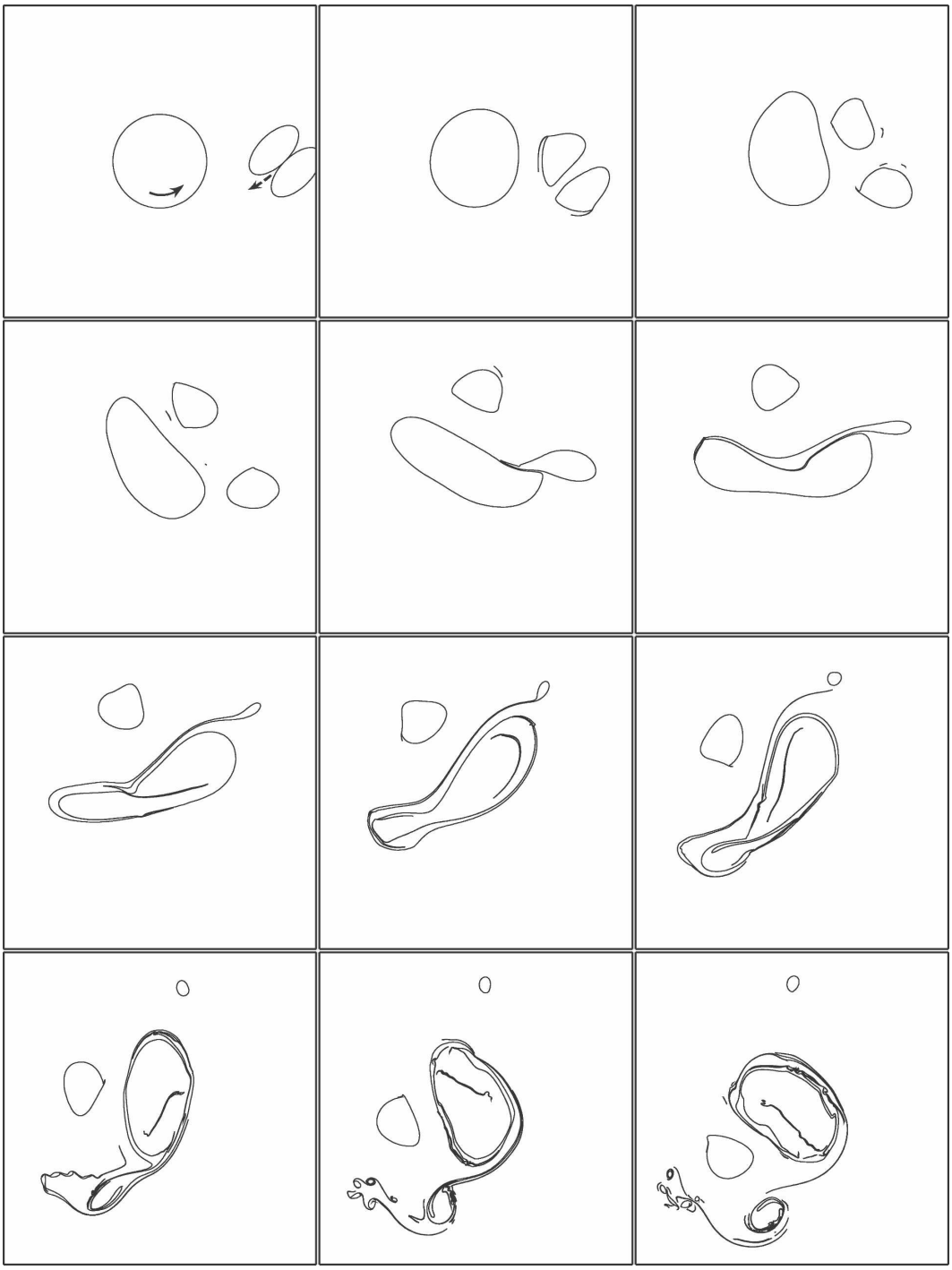

FIG. 2. Near-threshold barrier-penetration experiment (see section 3), viewed from above the North Pole of the model stratospheric polar vortex in the unbounded tangent-plane model. Time increases rightward then downward by increments $4\pi/\Delta q_{\text{barrier}}$, where $\Delta q_{\text{barrier}}$ is the quasigeostrophic PV contrast between the polar vortex and the surf zone. The angle of incidence is 225° initially. The solid arrow shows the sense of the polar vortex, and the dashed arrow shows the initial propagation of the vortex pair toward it. The vortex pair has relative strength exactly ± 1.0, where "relative strength" means $\Delta q_{\text{vortex}}/\Delta q_{\text{barrier}}$.

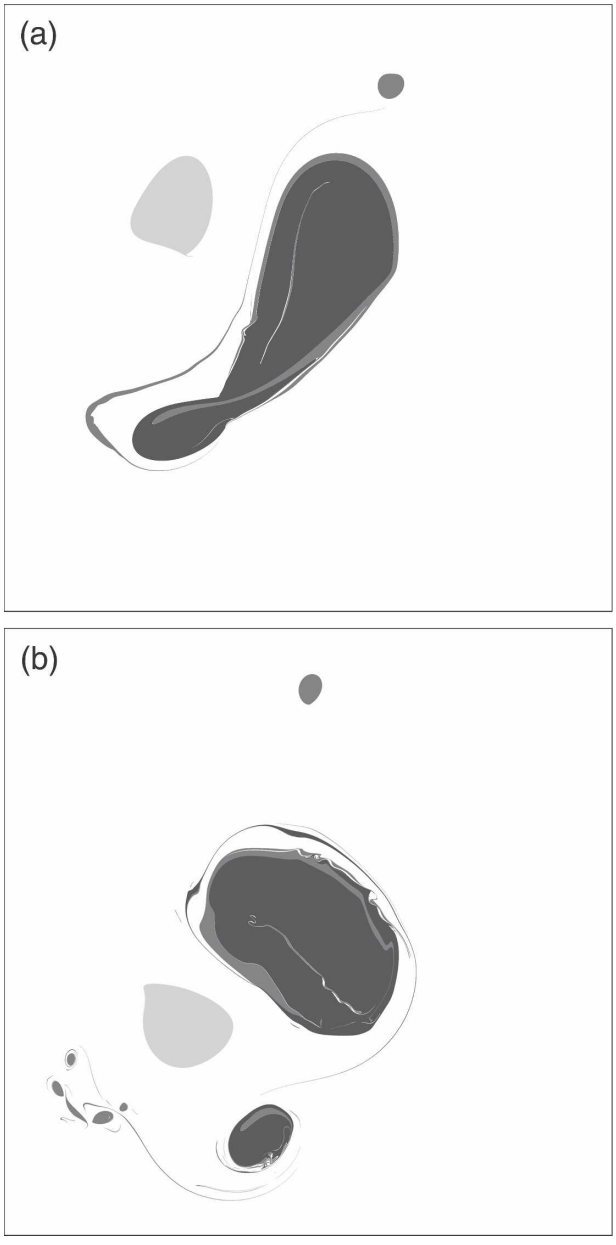

FIG. 3. High-resolution views of (a) the 9th and (b) the 12th panels of Fig. 2 (i.e., at times $32\pi/\Delta q_{\text{barrier}}$ and $44\pi/\Delta q_{\text{barrier}}$). The grayscaling distinguishes material from the ambient surf zone (white), the incident anticyclone (light gray), the incident cyclone (medium gray), and the polar vortex (darkest). Note that the last two shades have the same PV values, since Δq_{vortex} and $\Delta q_{\text{barrier}}$ are equal in this case.

following Bell (1990) that even without the boost from vortex-pair propagation, lone cyclones can also approach and penetrate the barrier, even a straight barrier, through a much slower and more subtle wave–vortex interaction related to classic vortex-merging dynamics. The thresholds themselves are hardly changed, except that the threshold values of $|\Delta q_{\text{vortex}}/\Delta q_{\text{barrier}}|$ become somewhat higher, typically by factors of 2–3, in the peripheral cases with core sizes substantially different from L_D. These are preliminary results only, for the purposes of illustration, and we hope to present a more systematic study in due course.

It might be asked why naturally occurring vortices in staircases are usually below threshold. At least, vortices are seldom if ever seen to cross an eastward jet either on Jupiter or in the terrestrial winter stratosphere. The answer could be that if such crossing events had ever been common they would already have broken some of the barriers, and thus widened the steps of the staircase until the barrier strengths, as measured by their PV contrasts, became comparable to or greater than those of the strongest vortices. The vortex strengths will of course be subject to some limitation arising from whatever stirring mechanism is in operation. If that mechanism, with accompanying radiation stresses as needed, is strong enough and effective enough to have created the staircase in the first place—arguably the situation on Jupiter—then the range of available vortex strengths will influence the step size such that the strongest vortices are only just below the threshold. Of course if the staircase is formed by Rossby wave breaking alone, then its strongest vortices initially have the same strengths as the material eroded from the barrier, which is automatically at or below the threshold.

4. Some decay experiments that illustrate the PV Phillips effect

To the extent that the PV Phillips effect is generic, it ought to be possible to demonstrate the resulting tendency toward inhomogeneous PV mixing in turbulence-decay experiments, with initial conditions statistically uniform in y.

Of course many such experiments have been done in the past, including the original Rhines (1975) experiments, but for various reasons (including early limitations on numerical resolution, and the privileging of power-spectral diagnostics over, e.g., PV maps) there has not always been a clear distinction between persistent jets produced by inhomogeneous PV mixing on the one hand and transient, migrating jets in the form of zonally long Rossby waves on the other. Also, both computer power and new numerical techniques now provide an opportunity to carry out such experiments at Reynolds numbers and effective resolutions vastly higher than before.

To our knowledge, however, a systematic study has yet to be completed at the level of today's state of the art. One reason is the difficulty of getting beyond the

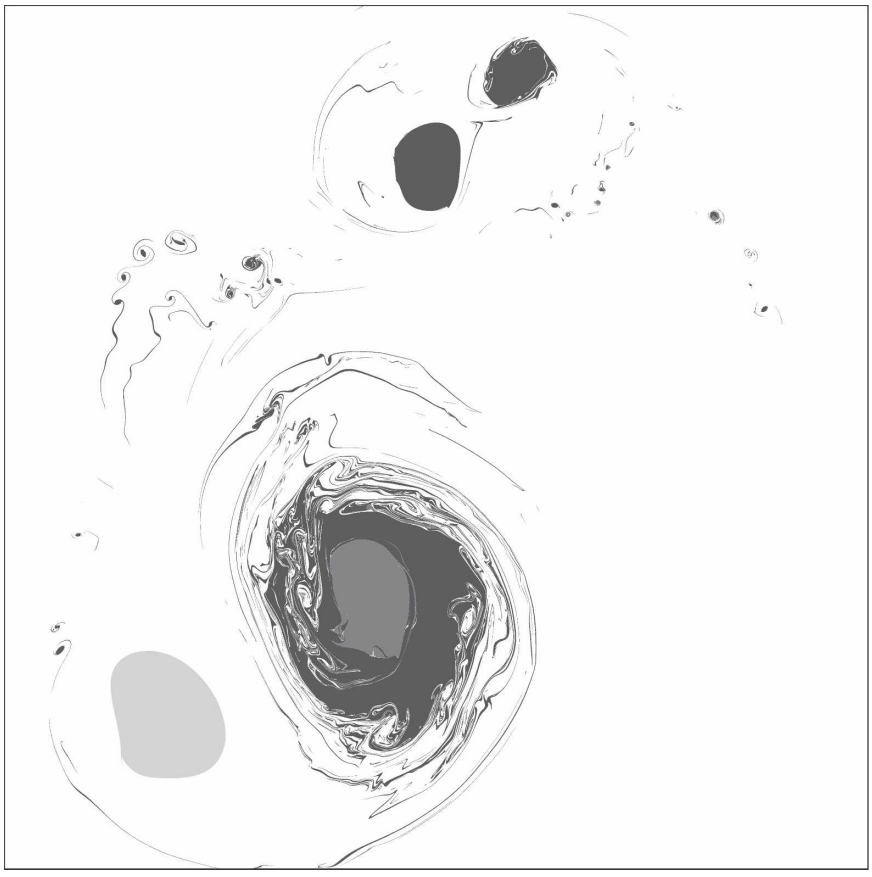

FIG. 4. Case of an incident vortex pair like that in Fig. 2, except with relative strength ± 1.4 instead of ± 1.0. Snapshot is at time $60\pi/\Delta q_{\text{vortex}}$, equivalently $60\pi/1.4\Delta q_{\text{barrier}}$. The incident cyclone (medium gray) has ended up almost entirely inside the polar vortex. The incident anticyclone (light gray) remains outside, as before. The remaining material outside is almost entirely from the polar vortex (darkest shading).

simple positive-feedback heuristic and of quantifying the wave–turbulence interplay in this situation, including the role of Rossby wave radiation stresses. In the present review, therefore, we limit ourselves to just one illustrative example that shows the PV Phillips effect particularly clearly. The example is taken from an ongoing series of numerical experiments to be reported elsewhere. These simulate freely decaying quasigeostrophic shallow-water turbulence in a beta-plane channel, starting with random vortices on an approximately uniform background PV gradient β. The experiments use a very accurate "contour-advective semi-Lagrangian" (CASL) algorithm (Dritschel and Ambaum 1997; Dritschel et al. 1999) able to simulate extraordinarily complex ultrahigh Reynolds number flows with great efficiency.

Not all such experiments provide equally clear illustrations of the PV Phillips effect. The tendency for PV mixing to be inhomogeneous is always seen, but has been found to range from very weak to very strong depending upon parameter values. The dependence is not only upon the background PV gradient and initial turbulent energy but also, more sensitively than we had expected, upon the Rossby length L_D. This may well be bound up with variations in the radiation-stress field related to variations in Rossby wave excitation and dispersion.

The experiment shown here is conducted in a channel of nondimensional width and length 2π with $L_D = 1$. Free-slip boundary conditions apply at $y = \pm\pi$, and the flow is periodic in x (see Benilov et al. 2004 for the use of the CASL algorithm in this geometry). The initial quasigeostrophic PV field q is built from a random anomaly field q' of maximum amplitude $|q'|_{\max} = 4\pi$ superposed on a linear background PV gradient βy, with $\beta = 2\pi$. The PV anomaly is correlated over a length ≈ 0.28; more precisely, the autocorrelation function of the PV-anomaly distribution has a roughly

Gaussian shape with a full width at half maximum of 0.28. The full PV (background plus anomaly) is discretized into steps with an initial mean step width $\Delta y = \pi/16 \approx 0.196 \approx L_D/5$, corresponding to a small PV jump $\Delta q_{\text{discrete}} = (2\pi)^2/31 \approx 1.27$ across each contour [a tiny fraction of the total planetary PV contrast across the width of the channel, $2\pi\beta = (2\pi)^2 \approx 39.5$]. The Eulerian grid resolution used to invert the PV to find the velocity field is 256×257; however, the PV is represented in a Lagrangian way, as contours, to permit highly accurate advection.

To deal with the turbulent dissipation of fine-grain PV gradients, surgery is applied at a twentieth of the Eulerian grid size (i.e., at the scale $\delta \approx 0.00123$). This apparent mismatch in the smallest scales used to represent the velocity and PV fields is justified (Dritschel and Ambaum 1997; Dritschel et al. 1999; Dritschel and Viúdez 2003, and references therein) by the steeper spectral decay of velocity fluctuations with decreasing scale.

Figure 5 shows the PV field at several stages in the flow evolution. The grayscale shading is sawtooth linear to make the detailed structure more visible. The flow rapidly grows in complexity, as measured by the total number of nodes on the contours. The complexity peaks at dimensionless time $t = 14$ (the unit of time being defined as $4\pi/|q'|_{\max}$). At that time, there are over seven million contour nodes. The complexity thereafter gradually decays as the flow becomes increasingly zonal. The PV Phillips effect is plainly in evidence in this case. Despite the statistical homogeneity of the initial conditions, the background PV field has been mixed in a highly inhomogeneous way.

This is seen even more clearly in Fig. 6, whose left-hand panel shows the time evolution of the mean y position of those PV contours that wrap the domain periodically in the x direction. As expected from the positive-feedback heuristic, the contours are pushed apart in some regions and squeezed together in others. The corresponding jets are evident in the right-hand panel of Fig. 6, which shows the zonally averaged zonal velocity $\overline{u}(y, t)$ at the initial and final times $t = 0$, 84.

5. Staircase inversions and jet spacing

The jet profiles in the right-hand panel of Fig. 6 may be compared, and contrasted, with the theoretical velocity profiles $u(y)$ for perfect PV staircases on an unbounded beta-plane. The theoretical expressions, obtained by PV inversion, are given in (5.1) and the following text and in (5.3), (5.5), and (5.6). Some examples are plotted in Fig. 7. For instance, the second curve from the left shows the $u(y)$ profile for a single step cut into the uniform background PV gradient, in the form of a perfectly mixed zone $|y| \le b$ of width $2b$, in the case $b = L_D$. The leftmost curve shows the corresponding mass shift expressed as the surface elevation change $h(y) = f_0\psi/g$, where g is gravity and f_0 a constant representative value of the Coriolis parameter. This mass shift is dictated by geostrophic balance with $u(y) = -\partial\psi/\partial y$. Notice that a smoothed version of the $u(y)$ curve qualitatively resembles the difference between the two velocity curves in Fig. 1b.

For general L_D, the $u(y)$ and $h(y)$ profiles within the single mixed zone $|y| \le b$ are given by

$$u(y) = \beta L_D^2\left[-1 + \left(1 + \frac{b}{L_D}\right)\exp\left(\frac{-b}{L_D}\right)\cosh\left(\frac{y}{L_D}\right)\right] \quad \text{for} \quad |y| \le b, \tag{5.1}$$

joining continuously to exponential tails $\propto \exp(-|y|/L_D)$ on each side $|y| > b$ (Fig. 7b) and, with $H_0 = f_0^2 L_D^2/g$, the undisturbed layer depth,

$$h(y) = \frac{\beta L_D H_0}{f_0}\left[\frac{y}{L_D} - \left(1 + \frac{b}{L_D}\right)\exp\left(\frac{-b}{L_D}\right)\sinh\left(\frac{y}{L_D}\right)\right] \quad \text{for} \quad |y| \le b, \tag{5.2}$$

with values and first derivatives joining continuously to side tails $\propto \exp(-|y|/L_D)$ in $|y| > b$ (Fig. 7a). The last three curves in Fig. 7 are the $u(y)$ profiles for staircases of two, three, and an infinite number of steps or mixed zones, constructed by the appropriate daisychaining of (5.1), that is, by superposition of laterally shifted copies of (5.1) and its side tails. Superposition is allowed because quasigeostrophic β-plane PV inversion (3.2), with f now variable but L_D still constant, is a linear operation. The limiting case of the perfect periodic staircase, uniquely determined by construction as an infinite daisy chain, has profiles that are readily shown to be

$$u(y) = \beta L_D^2\left[-1 + \frac{b}{L_D}\frac{\cosh(y/L_D)}{\sinh(b/L_D)}\right] + \text{periodic extension} \tag{5.3}$$

and

$$h(y) = \frac{\beta L_D H_0}{f_0}\left[\frac{y}{L_D} - \frac{b}{L_D}\frac{\sinh(y/L_D)}{\sinh(b/L_D)}\right] + \text{periodic extension.} \tag{5.4}$$

The expressions shown explicitly are valid in $|y| \le b$, representing (5.1) and (5.2) plus infinite sums of side tails from the other zones. The rightmost curve in Fig. 7 is (5.3) shifted laterally by a distance b.

In the rigidly bounded, nondivergent barotropic limit

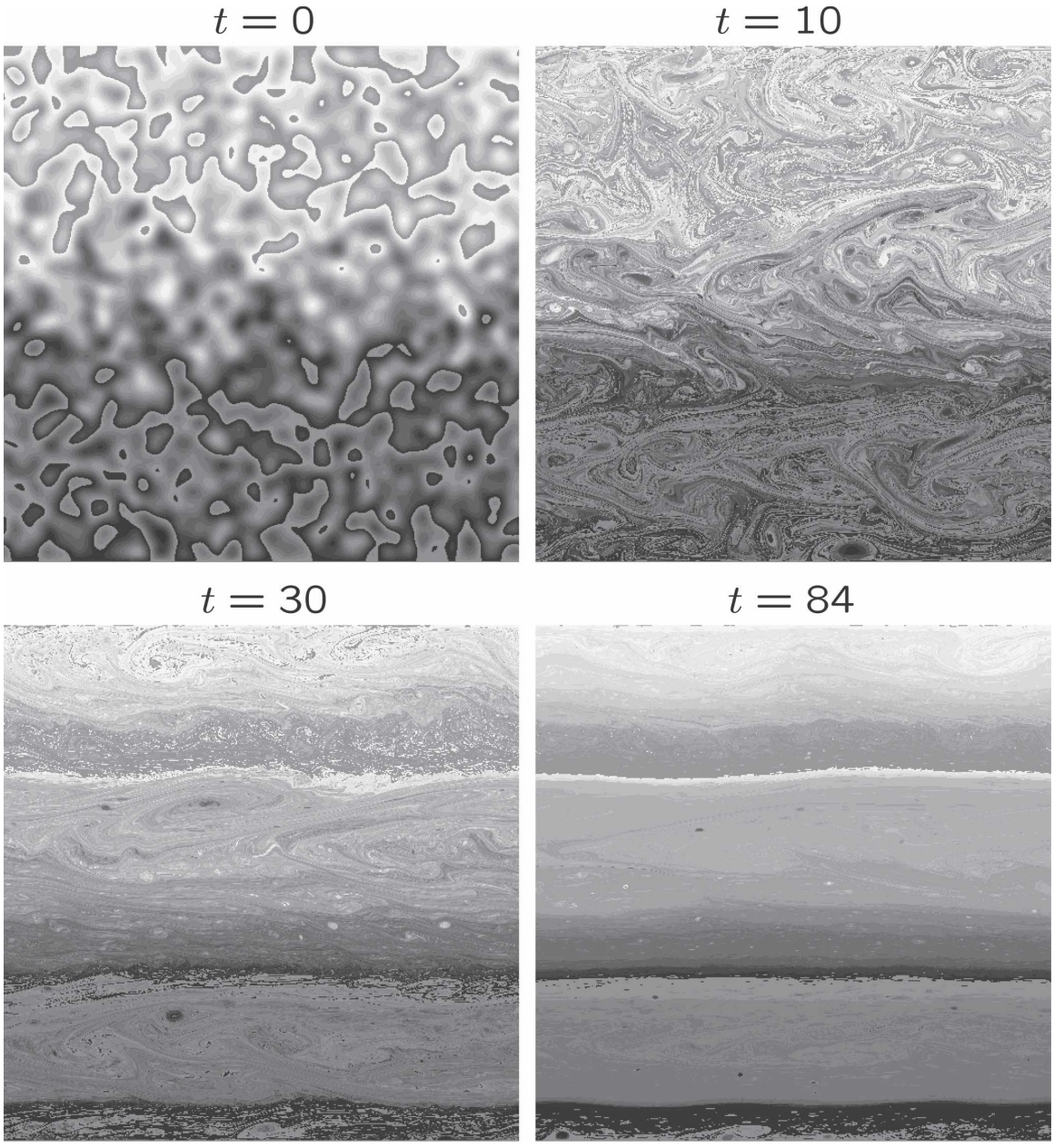

FIG. 5. Simulation of a quasigeostrophic shallow-water turbulent flow in a channel (see section 4). Time evolves to the right and downward, as labeled in units of $4\pi/|q'|_{\max}$. That is, the eddy turnaround time is unity for the initial maximum PV anomaly.

$L_D/b \to \infty$, (5.1) and (5.3) become, respectively, with fractional error $O(b/L_D)^3$,

$$u(y) \approx \frac{1}{2}\beta(y^2 - b^2) \quad \text{for} \quad |y| \le b, \tag{5.5}$$

and

$$u(y) \approx \frac{1}{2}\beta\left(y^2 - \frac{1}{3}b^2\right) + \text{periodic extension}, \tag{5.6}$$

a daisy chain of parabolas. Note that this is a case of noninterchangeable limits. Equation (5.6) is not the result of daisychaining (5.5), because the infinite daisy chain limit is not interchangeable with the limit $L_D/b \to \infty$. The reason is that the side tails of the single-zone solution (5.5) are infinitely weak and infinitely broad but contain finite relative angular momentum. We discuss the corresponding absolute angular-momentum changes in section 7 below. The staircase found by Danilov and Gurarie (2004) and Danilov and Gryanik

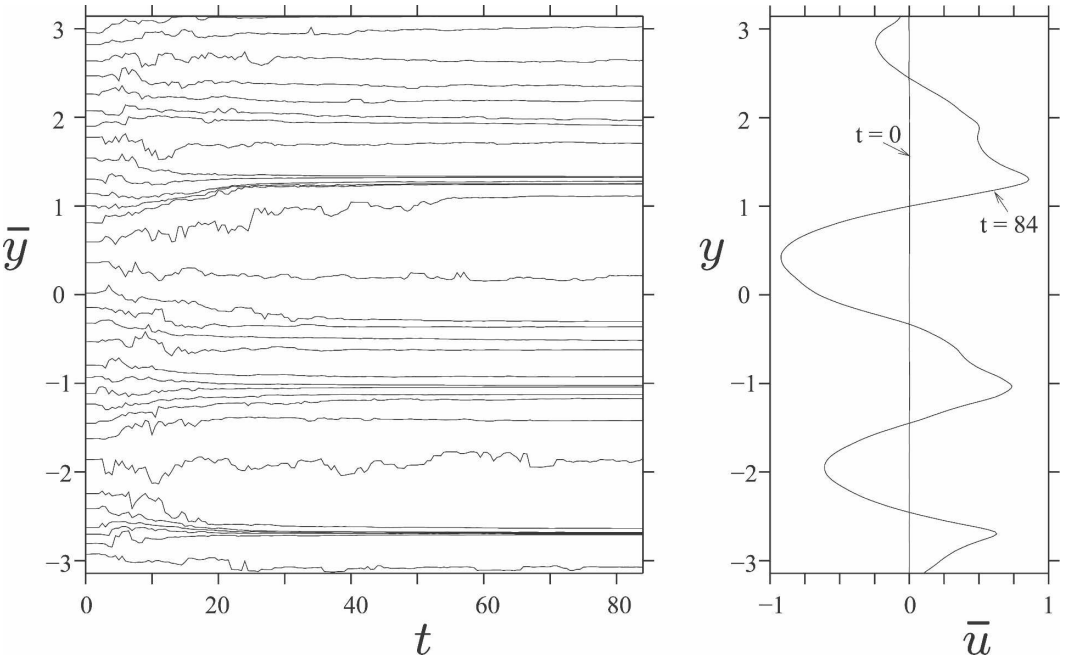

FIG. 6. Diagnostics for the experiment of Fig. 5. The left-hand panel shows the time evolution of the zonal-mean position $\bar{y}(q, t)$ of each PV contour that wraps the domain (i.e., that closes on itself only through the periodic boundaries $x = \pm\pi$). The latitudinal coordinate y is in units of L_D, and time t is in units of $4\pi/|q'|_{\max}$. PV mixing (in which the turbulent dissipation of fine-grain PV gradients is achieved here by contour surgery) changes $\bar{y}(q, t)$ in time, here leading to a highly inhomogeneous distribution of positions $\bar{y}$ at late times, as expected from the positive-feedback heuristic. Broadly speaking, the bunching of curves corresponds to eastward jet formation and the spreading of curves to westward jet formation. The right-hand panel shows the zonally averaged zonal velocity $\bar{u}(y, t)$ at the initial and final times $t = 0, 84$. (See remark at the end of section 7.) The inhomogeneous PV mixing has produced three strong eastward jets, two of them sharply peaked in the manner characteristic of well-developed eddy-transport barriers in a shallow-water system, with PV distributions close to jump discontinuities. Such PV distributions invert to velocity profiles locally resembling the idealized forms shown in Fig. 7, which correspond to perfectly sharp PV jump discontinuities.

(2004) in their rigidly bounded barotropic turbulence model produces (5.6) almost exactly, apart from an additive constant.

For all values of L_D/b these examples show the generic feature of sharply peaked eastward jets with broad westward flows in between, the more so in cases with small L_D/b. This asymmetry has often been remarked on. From (5.1) and (5.3) it is evident that for small L_D/b the eastward jets are thinner and still more sharply peaked, with width scale L_D, and the intervening westward flows relatively still more broad.

The inversions (5.1) and (5.3) assume straight jets. Recent work on shallow-water flows with a latitudinal variation of L_D like that expected on Jupiter (e.g., Theiss 2004; Scott and Polvani 2007), following ideas of Salmon (1982), suggest that for the smaller values of L_D, as in modeling Jupiter's high latitudes, the jets not only become thinner but meander strongly as well, while keeping themselves sharp. This is also reminiscent of many terrestrial ocean currents (e.g., Niiler et al. 2003). It is probably related to the relative "sloppiness" of vortex interactions at small L_D (e.g., Waugh and Dritschel 1991) and to the smooth, stable behavior of large-amplitude long Rossby waves on jets like (5.1) or (5.3) at small L_D (Nycander et al. 1993). Of course in some cases the meanders may be due to, or increased by, baroclinic instability, as with atmospheric tropopause jets, taking us outside the scope of barotropic shallow-water modeling.

It is worth emphasizing that the Rossby elasticity and hence the Rhines and Phillips effects cannot be expected to be negligible even in the limit $L_D \to 0$. The wave–turbulence interplay is still inescapable. Rossby waves on thin jets have phase speeds of the same order as the jet velocity scale. Therefore, in the staircase scenario with vortex cores of size $\sim L_D$, jet widths $\sim L_D$, and eddy velocities of the same order as jet velocities, the order-of-magnitude regime is just that usually associated with the Rhines effect understood as "cascade arrest" or "cascade retardation" in wavenumber space,

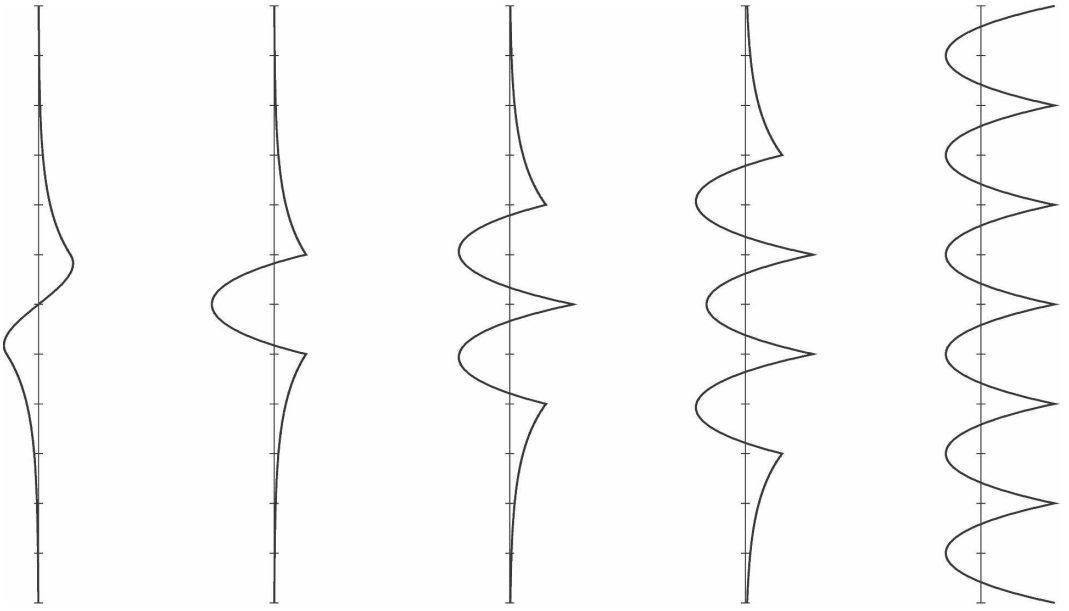

FIG. 7. Idealized mass and velocity profiles for perfect PV staircase steps, as determined by PV inversion. Tick marks are at intervals of $y = b = L_D$. From left to right, the first two profiles are for a single step or mixed zone, respectively the mass shift or surface elevation change given by (5.2) ff. and the velocity profile given by (5.1) ff. The remaining profiles are the velocity profiles for two, three, and an infinite number of perfect steps, the last from Eq. (5.3) shifted by b. Note that the angular momentum changes required to form these staircase structures are nonvanishing, and are precisely dictated by the PV inversions, or equivalently by Eq. (7.2).

or simply as "Rossby elasticity significant" or "waves and turbulence both significant," at the length scale L_D. For instance in the thin-jet limit $L_D \to 0$ with b finite it is well known, and readily shown, that Rossby waves on the jet (5.3) near $y = b$, say, all have phase speeds c lying between maximum u and minimum u. This means not only that Rossby elasticity is significant but also that there are critical layers in the jet flanks—implying a two-sided version of Fig. 1—hence, in reality, surf zones that would mix PV there had it not been mixed already and the jet already sharpened. Hughes (1996) discusses this further. Once again we have turbulence intimately and inescapably associated with waves, the essence of the Rhines effect.

6. Rhines scales versus jet spacing

Even a cursory perusal of the literature shows that the term "Rhines scale" is used with a plethora of meanings; see, for instance, Dunkerton and Scott (2008), who consider three different length scales, which they call "dynamical Rhines scale," "spectral Rhines scale," and "geometric Rhines scale." Some authors even define Rhines scale such that it can "fail to exist" as a real number. Others appear to assume that it always means the jet spacing.

Without presuming to say what the term "should" mean, in a given dynamical context, we choose to define the Rhines scale here in its simplest possible sense. If a velocity scale U is given, or arises naturally (as in the staircase problem), then dimensional analysis tells us that one of the length scales in the problem must be $(U/\beta)^{1/2}$, where β is the planetary absolute vorticity gradient. We call this the Rhines scale based on U, and use the symbol $L_{\mathrm{Rh}}(U)$ to denote simply that length scale, by definition, recognizing of course that different velocity scales U will arise and that the length scale $L_{\mathrm{Rh}}(U)$ may or may not turn out to have a visible role in one or another dynamical regime, viewed spectrally or in any other way.

The Rhines scales $L_{\mathrm{Rh}}(U_{\mathrm{vortex}})$ and $L_{\mathrm{Rh}}(U_{\mathrm{jet}})$ based respectively on vortex peak velocity U_{vortex} and jet velocity $U_{\mathrm{jet}} = (\max u - \min u)$ are accordingly defined by

$$L^2_{\mathrm{Rh}}(U_{\mathrm{vortex}}) = U_{\mathrm{vortex}}/\beta, \quad L^2_{\mathrm{Rh}}(U_{\mathrm{jet}}) = U_{\mathrm{jet}}/\beta. \tag{6.1}$$

For our standard case of vortex core size $\sim L_D$, and assuming $b \gtrsim L_D$ such that there is room for the vortices between the jets, the threshold relation (3.3) tells us that $\Delta q_{\mathrm{vortex}} \sim \Delta q_{\mathrm{barrier}} \sim \beta b$. The inversions (5.1) and (5.3) tell us that the jet velocity-profile width scale is L_D in this case. It follows that $U_{\mathrm{jet}} \sim L_D \Delta q_{\mathrm{barrier}} \sim$

$L_D\beta b \sim L_D\Delta q_{\rm vortex} \sim U_{\rm vortex}$, and therefore $L_{\rm Rh}(U_{\rm jet}) \sim L_{\rm Rh}(U_{\rm vortex})$ and

$$b \sim L^2_{\rm Rh}(U_{\rm vortex})/L_D. \tag{6.2}$$

So the Rhines scale as defined here is not always the same as the jet spacing, though the two length scales coincide when $L_D/b \sim 1$.

For vortex-core sizes differing substantially from L_D, the scaling is less simple. This is both because the thresholds are then somewhat higher than (3.3) and because, for vortices of given strength $\Delta q_{\rm vortex}$ but core size $\ll L_D$, the scaling $U_{\rm vortex} \sim \Delta q_{\rm vortex} L_D$ is replaced by $U_{\rm vortex} \sim \Delta q_{\rm vortex} \times$ core size. However, we still have a simple relation between b, L_D, and $L_{\rm Rh}(U_{\rm jet})$ across the whole range of parameter conditions. By putting (6.1) together with (5.3) we get

$$\left[\frac{L_{\rm Rh}(U_{\rm jet})}{L_{\rm D}}\right]^2 = \frac{b}{L_D}\frac{\cosh(b/L_D)-1}{\sinh(b/L_D)} = \frac{b}{L_D}\tanh\left(\frac{b}{2L_D}\right). \tag{6.3}$$

Figure 8 shows the implied relation between the jet spacing $2b$ and $L_{\rm Rh}(U_{\rm jet})$. The left-hand portion of the graph gives us the standard result $b \sim L_{\rm Rh}(U_{\rm jet})$ for $L_D/b \gtrsim 1$, while the right-hand portion recovers the behavior (6.2) for $L_D/b \lesssim 1$.

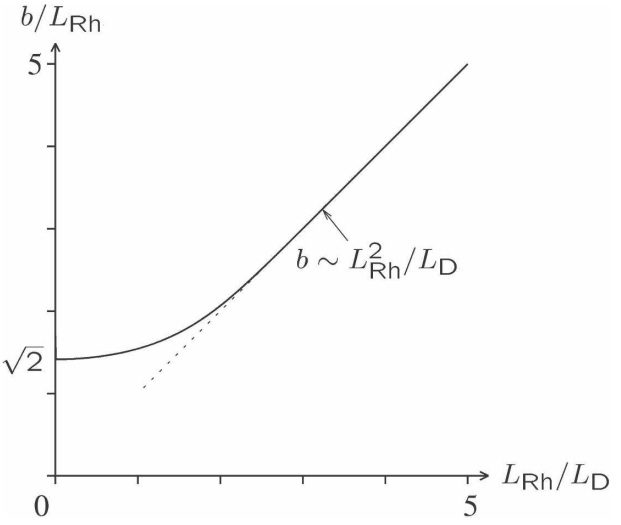

FIG. 8. Relation between jet spacing $2b$ in a perfect periodic staircase and Rhines scale $L_{\rm Rh} = L_{\rm Rh}(U_{\rm jet})$ based on jet velocity, for different values of the Rossby length $L_{\rm D}$, from Eq. (6.3) rewritten in parametric form as $(L_{\rm Rh}/L_D,\ b/L_{\rm Rh}) = \{s^{1/2}[\tanh(s/2)]^{1/2},\ s^{1/2}[\tanh(s/2)]^{-1/2}\}$ where $s = b/L_D$ runs over positive values. The relation plotted is an immediate consequence of PV inversion as shown by Eq. (5.3).

7. Angular momentum changes due to PV mixing

The PV invertibility principle tells us that a PV mixing event localized in y will produce a definite and unambiguous total angular momentum change δM. The single-zone inversion (5.1)–(5.2) illustrates that fact very clearly, as will be shown next. It is one way of seeing that radiation stresses—most directly and simply those associated with Rossby wave radiation—must inevitably be associated with PV mixing as also shown by the Taylor identity (see appendix). It also suggests that PV mixing may be catalyzed by the stresses due to other wave types.

Consider a conservative PV mixing event like that required to create a single staircase step or surf zone, in which the PV is changed by $\delta q(y)$ where $\int \delta q(y)\,dy = 0$. For the case of a perfectly mixed step created from a uniform background PV gradient β, the profile $\delta q(y)$ is N-shaped with slope $-\beta$. Inverting it gives the $u(y)$ profile (5.1) and the $h(y)$ profile (5.2). The associated angular momentum change, δM, can be shown as follows to be proportional to $\int y\delta q(y)\,dy$, which is generically nonzero [e.g., $-\frac{2}{3}\,\beta b^3$ for the N-shaped $\delta q(y)$].

For the unbounded beta-plane model, in which the distance to the rotation axis is infinite, it is natural to define δM as the change in absolute zonal momentum per unit x distance. For our shallow-water layer of undisturbed depth H_0 and, say, constant mass density ρ_0, the absolute zonal momentum per unit horizontal area is $\rho_0[H_0 + h(y)][u(y) - f_0 y]$, which to quasigeostrophic accuracy is changed by $\rho_0 H_0 \delta u(y) - \rho_0 f_0 y \delta h(y)$ when u changes by $\delta u(y)$ and h by $\delta h(y)$ so that, with

$$\delta u = -\partial(\delta\psi)/\partial y, \tag{7.1}$$

$$\begin{aligned}\delta M &= \rho_0 \int_{-\infty}^{\infty} [H_0\delta u(y) - f_0 y \delta h(y)]\,dy \\ &= \rho_0 H_0 \int_{-\infty}^{\infty} \left[-\frac{\partial(\delta\psi)}{\partial y} - L_D^{-2} y \delta\psi\right] dy \\ &= \rho_0 H_0 \int_{-\infty}^{\infty} y\left[\frac{\partial^2(\delta\psi)}{\partial y^2} - L_D^{-2}\delta\psi\right] dy \\ &= \rho_0 H_0 \int_{-\infty}^{\infty} y\delta q(y)\,dy. \end{aligned} \tag{7.2}$$

The last expression has an alternative interpretation as the *Kelvin impulse* for the quasigeostrophic system. For its general conservation relation see, for example, Bühler and McIntyre (2005, section 8).

Notice from the steps leading from (7.1) to (7.2) that all the angular momentum change is in the mass shift and none in the relative velocity since $\delta u = -\partial(\delta\psi)/\partial y$, which integrates to zero by virtue of the evanescence of the PV inversion-operator kernel, K_0. That evanescence is reflected, for instance, in the exponential decay

of the side tails of $h(y) = f_0\psi/g$ associated with (5.2). The fact that all the angular momentum change is in the mass shift is one of the peculiarities of quasigeostrophic theory. So a check on the correctness of (5.2) is to multiply it by y and integrate (including the side tails), whereupon one finds that all the terms in L_D cancel, as they must for consistency with (7.2) and the fact that the N-shaped $\delta q(y)$ profile is independent of L_D. Specifically,

$$\delta M = -\frac{2}{3}\rho_0 H_0 \beta b^3 \tag{7.3}$$

for the perfectly mixed step or surf zone. An alternative derivation of the general result (7.2) is to integrate the Taylor identity (A.1) with respect to y and t across the PV mixing event.

We note in passing that channel and y-periodic numerical beta-plane models may have artificial constraints on their absolute momentum, which may suppress or modify the globally integrated δM changes just discussed. However, such artificiality is a price often worth paying for numerical power and convenience.

8. Concluding remarks

The PV staircase, an extreme case of the inhomogeneity encouraged by the PV Phillips effect, can arise when stirring is strong provided also that it is accompanied by a suitable radiation-stress field.

One of the simplest examples of such a stress field is that described in connection with Fig. 1, where Rossby waves propagate upward on the jet axis, setting up a vertical Eliassen–Palm (EP) flux or form stress (A.2) (see note 1), and then refract and break to one or both sides of the jet causing PV mixing on its flanks. That is one way to satisfy the Taylor identity, (A.3) below, illustrating how breaking Rossby waves tend to be efficient at PV mixing and to produce the familiar antifrictional $\overline{u'v'}$ patterns described variously as trailing troughs, herringbone patterns, chevron shapes, and so on.

On Jupiter, we may speculate that the eastward jets may similarly carry upward-propagating Rossby waves as a significant part of the whole wave–turbulence jigsaw, helping the stirring and PV mixing on either side to be efficient, and keeping the associated eddy-transport barriers, acting as Rossby waveguides, as tight as the observations suggest they are in reality. The eastward jets may well have significant roots in the thermally convecting interior, by virtue of the Taylor–Proudman effect (expanding Rossby height as the static stability evanesces beneath the stably stratified cloud layers). Jostling or nudging by large, ponderous convective eddies, beneath the clouds, could be a significant source of upward-propagating Rossby waves on those jets and could take the place of baroclinic instability (see note 4) as the excitation mechanism whose radiation stress catalyzes the PV mixing aloft.

Many terrestrial ocean jets can similarly be excited, and thus self-sharpen, even when not baroclinically unstable (e.g., Hughes 1996). This is because such jets often feel the bottom topography.

Complementing this picture are the barrier-penetration experiments of section 3, for established staircases, and the decaying-turbulence experiments of section 4 and Figs. 5–6 to investigate the Phillips effect. Both are in their infancy, and we make no pretence to having done a definitive study in either case. We have done no more than describe a few examples in the hope of illustrating and pulling together some generic points that are more or less well known. The issues thus highlighted are, however, a challenge for future work. The results are suggestive, particularly the simple barrier-penetration threshold (3.3) that is found for the most effective vortices and vortex pairs, with core sizes on the order of the Rossby length L_D. In three-dimensional, fully stratified problems, such vortices correspond to those having core aspect ratios on the order of Prandtl's ratio f/N, where N is the buoyancy frequency of the stratification. It is precisely such vortices that are the most robust and stable according to a number of recent studies (e.g., Reinaud et al. 2003 and references therein).

In the experiments of section 4 we found a large range of cases from weakly to strongly inhomogeneous PV mixing, the latter illustrated by Fig. 6. Progress in understanding them is bound to depend on finding ways to analyze and quantify the Rossby wave radiation-stress field that must coexist with the decaying turbulence and catalyze PV mixing to varying degrees—another challenge for the future, especially as we extend the work prior to attempting realistic forced experiments that try to establish quasi-Jovian PV staircases.

Finally, we note again that once a PV staircase is established with step widths $\gtrsim L_D$, along with stirring by the most effective vortices (core sizes $\sim L_D$), the threshold (3.3) and the PV inversion results of section 5 together imply that the "turbulent" Rhines scale $L_{\mathrm{Rh}}(U_{\mathrm{vortex}})$ is related to the jet spacing or staircase step width $2b$ by

$$2b \sim L_{\mathrm{Rh}}^2(U_{\mathrm{vortex}})/L_D \tag{8.1}$$

in order of magnitude.

Acknowledgments. We thank the organizers for inviting us to such an interesting Chapman Conference,

in which the problems of multiple jets and annular modes were looked at from so many different angles, for the various terrestrial and extraterrestrial cases. A number of colleagues have helped us with stimulating comments on this work and in other ways, in particular Michael Allison, Pavel Berloff, Sergey Danilov, Huw Davies, Timothy Dunkerton, Boris Galperin, Peter Haynes, Christopher Hughes, John Lewis, Nili Harnik, Philip Marcus, Nikolai Maximenko, Robb McDonald, George Platzman, Peter Rhines, John Rogers, Richard Scott, Sushil Shetty, Emily Shuckburgh, Roger Smith, Jürgen Theiss, Geoffrey Vallis, John M. Wallace, William R. Young, and the reviewers of this paper.

APPENDIX

The Taylor Identity

The well-known Taylor identity is valid for fully nonlinear quasigeostrophic motion, and has central importance by virtue of the way in which it relates PV fluxes, due for instance to PV mixing, to Rossby wave radiation-stress divergences. For the quasigeostrophic shallow-water model it reads

$$\overline{v'q'} = -\frac{\partial}{\partial y}\overline{u'v'}. \tag{A.1}$$

The overbar denotes the zonal average as before and primes denote departures from it. The identity follows readily from the relations $(u', v') = (-\partial\psi'/\partial y, \partial\psi'/\partial x)$ and $q' = \mathcal{L}(\psi') = (\nabla^2 - L_D^{-2})\psi'$, the quasigeostrophic shallow-water PV anomaly. The term in L_D averages to zero. The original version noted and used by Taylor (1915) and Kuo (1951) was for the limit $L_D \to \infty$, that is, for rigidly bounded, barotropic nondivergent vortex dynamics.

The generalization to three-dimensional quasigeostrophic dynamics is noted here for completeness. It first appeared in print in Bretherton (1966a, p. 329) and has also been attributed to Eady via Green (1970). The Rossby wave radiation stresses are quantified as Eliassen–Palm fluxes whose meridional, y, and vertical, z, components, with the standard sign convention (such that flux directions correspond to Rossby wave group velocities when applicable), are

$$(F, G) = \rho_0(z)(-\overline{u'v'}, f_0\overline{v'\theta'}/N^2), \tag{A.2}$$

where θ is the buoyancy acceleration, N the buoyancy frequency, $\rho_0(z)$ a background density $\propto \exp(-z/H_{\rm scale})$, and f_0 a constant nominal value of the Coriolis parameter as before. The vertical component G is the form stress. Then the Taylor identity becomes

$$\overline{v'q'} = \frac{1}{\rho_0}\left(\frac{\partial F}{\partial y} + \frac{\partial G}{\partial z}\right), \tag{A.3}$$

with the PV anomaly now defined as

$$q' = \frac{\partial^2\psi'}{\partial x^2} + \frac{\partial^2\psi'}{\partial y^2} + \frac{1}{\rho_0}\frac{\partial}{\partial z}\left(\frac{\rho_0 f_0^2}{N^2}\frac{\partial\psi'}{\partial z}\right). \tag{A.4}$$

Equation (A.3) follows in almost the same way as before, from the standard relations $(u', v', \theta') = (-\partial\psi'/\partial y, \partial\psi'/\partial x, f_0\partial\psi'/\partial z)$. The first-moment Eq. (7.2) for the absolute momentum or Kelvin impulse change continues to hold provided that, in the three-dimensional case, one replaces $\rho_0 H_0$ by $\rho_0(z)dz$ and integrates vertically as well as meridionally across the zone of PV mixing.

Consistently with (A.3), G/ρ_0 at a flat boundary representing an oceanic upper or atmospheric lower surface can be interpreted (Bretherton 1966a) as a boundary delta-function contribution to $\overline{v'q'}$, just above or beneath which G is set to zero on the boundary. Since at the boundary θ is approximately a material invariant, it is subject to mixing in the same way as the PV above the boundary, with the same dynamical significance for the wave–turbulence jigsaw and crucial, for instance, to the workings of linear and nonlinear baroclinic instability including the upward launch of Rossby waves in the first nonlinear stage of an LC1 baroclinic wave life cycle. The elegant work of Plumb and Ferrari (2005) extends the above to cases outside the scope of standard quasigeostrophic theory, able to encompass steeply sloping stratification surfaces in, for instance, oceanic mixed layers and atmospheric boundary layers. The appropriate set of generalized Taylor identities are presented in their Eqs. (22)–(27).

REFERENCES

Allison, M., 2000: A similarity model for the windy jovian thermocline. *Planet. Space Sci.,* **48,** 753–774.

Balmforth, N. J., S. G. Llewellyn-Smith, and W. R. Young, 1998: Dynamics of interfaces and layers in a stratified turbulent fluid. *J. Fluid Mech.,* **355,** 329–358.

Barenblatt, G. I., M. Bertsch, R. Dal Passo, N. V. M. Prostokishin, and M. Ughi, 1993: A mathematical model of turbulent heat and mass transfer in stably stratified shear flow. *J. Fluid Mech.,* **253,** 341–358.

Bell, G. I., 1990: Interaction between vortices and waves in a simple model of geophysical flow. *Phys. Fluids,* **A2,** 575–586.

Benilov, E. S., J. Nycander, and D. G. Dritschel, 2004: Destabilization of barotropic flows by small-scale topography. *J. Fluid Mech.,* **517,** 359–374.

Bretherton, F. P., 1966a: Critical layer instability in baroclinic flows. *Quart. J. Roy. Meteor. Soc.,* **92,** 325–334.

——, 1966b: Baroclinic instability and the short wavelength cutoff in terms of potential vorticity. *Quart. J. Roy. Meteor. Soc.,* **92,** 335–345.

——, 1969: Momentum transport by gravity waves. *Quart. J. Roy. Meteor. Soc.,* **95,** 213–243.

Bühler, O., and M. E. McIntyre, 2005: Wave capture and wave-vortex duality. *J. Fluid Mech.,* **534,** 67–95.

Danielsen, E. F., 1968: Stratospheric-tropospheric exchange based on radioactivity, ozone and potential vorticity. *J. Atmos. Sci.,* **25,** 502–518.

Danilov, S., and V. M. Gryanik, 2004: Barotropic beta-plane turbulence in a regime with strong zonal jets revisited. *J. Atmos. Sci.,* **61,** 2283–2295.

——, and D. Gurarie, 2004: Scaling, spectra and zonal jets in beta-plane turbulence. *Phys. Fluids,* **16,** 2592–2603.

Dickinson, R. E., 1969: Theory of planetary wave-zonal flow interaction. *J. Atmos. Sci.,* **26,** 73–81.

Dritschel, D. G., 1989: Contour dynamics and contour surgery: Numerical algorithms for extended, high-resolution modelling of vortex dynamics in two-dimensional, inviscid, incompressible flows. *Comp. Phys. Rep.,* **10,** 77–146.

——, and M. H. P. Ambaum, 1997: A contour-advective semi-Lagrangian numerical algorithm for simulating fine-scale conservative dynamical fields. *Quart. J. Roy. Meteor. Soc.,* **123,** 1097–1130.

——, and A. Viúdez, 2003: A balanced approach to modelling rotating stably-stratified geophysical flows. *J. Fluid Mech.,* **488,** 123–150.

——, L. M. Polvani, and A. R. Mohebalhojeh, 1999: The contour-advective semi-Lagrangian algorithm for the shallow water equations. *Mon. Wea. Rev.,* **127,** 1551–1565.

Dunkerton, T. J., and R. K. Scott, 2008: A barotropic model of the angular momentum conserving potential vorticity staircase in spherical geometry. *J. Atmos. Sci.,* **65,** 1127–1157.

——, and Coauthors, 1981: Some Eulerian and Lagrangian diagnostics for a model stratospheric warming. *J. Atmos. Sci.,* **38,** 819–843.

Eady, E. T., 1950: The cause of the general circulation of the atmosphere. *Centenary Proceedings,* P. A. Sheppard et al., Eds., Roy. Meteor. Soc., 156–172.

——, 1954: The maintenance of the mean zonal surface currents. *Proceedings of the Toronto Meteorological Conference,* T. W. Wormell et al., Eds., Roy. Meteor. Soc., 124–128.

Edmon, H. J., Jr., B. J. Hoskins, and M. E. McIntyre, 1980: Eliassen-Palm cross sections for the troposphere. *J. Atmos. Sci.,* **37,** 2600–2616; Corrigendum, **38,** 1115.

Eliasen, E., 1961: On the interactions between the long baroclinic waves and the mean zonal flow. *Tellus,* **13,** 40–55.

Fultz, D., R. R. Long, G. V. Owens, W. Bohan, R. Kaylor, and J. Weil, 1959: *Studies of Thermal Convection in a Rotating Cylinder with Some Implications for Large-Scale Atmospheric Motions. Meteor. Monogr.,* No. 4, Amer. Meteor. Soc., 104 pp.

Green, J. S. A., 1970: Transfer properties of the large-scale eddies and the general circulation of the atmosphere. *Quart. J. Roy. Meteor. Soc.,* **96,** 157–185.

Greenslade, M., and P. H. Haynes, 2008: Vertical transition in transport and mixing in baroclinic flows. *J. Atmos. Sci.,* **65,** 1158–1178.

Haynes, P. H., 1989: The effect of barotropic instability on the nonlinear evolution of a Rossby-wave critical layer. *J. Fluid Mech.,* **207,** 231–266.

——, 2005: Stratospheric dynamics. *Annu. Rev. Fluid Mech.,* **37,** 263–293.

——, and E. F. Shuckburgh, 2000: Effective diffusivity as a diagnostic of atmospheric transport. Part 1: Stratosphere. *J. Geophys. Res.,* **105,** 22 777–22 794.

——, and Coauthors, 1991: On the "downward control" of extratropical diabatic circulations by eddy-induced mean zonal forces. *J. Atmos. Sci.,* **48,** 651–678.

——, D. A. Poet, and E. F. Shuckburgh, 2007: Transport and mixing in kinematic and dynamically consistent flows. *J. Atmos. Sci.*, **64,** 3640–3651.

Held, I., 1975: Momentum transport by quasi-geostrophic eddies. *J. Atmos. Sci.,* **32,** 1494–1497.

Hide, R., 1958: An experimental study of thermal convection in a rotating liquid. *Philos. Trans. Roy. Soc. London,* **A250,** 441–478.

Hoskins, B. J., and Coauthors, 1985: On the use and significance of isentropic potential-vorticity maps. *Quart. J. Roy. Meteor. Soc.,* **111,** 877–946; Corrigendum, **113,** 402–404.

Huang, H.-P., B. Galperin, and S. Sukoriansky, 2001: Anisotropic spectra in two-dimensional turbulence on the surface of a rotating sphere. *Phys. Fluids,* **13,** 225–240.

Hughes, C. W., 1996: The Antarctic Circumpolar Current as a waveguide for Rossby waves. *J. Phys. Oceanogr.,* **26,** 1375–1387.

Hunt, J. C. R., and P. A. Durbin, 1999: Perturbed vortical layers and shear sheltering. *Fluid Dyn. Res.,* **24,** 375–404.

Ingersoll, A. P., 1976a: The atmosphere of Jupiter. *Sci. Amer.,* **234** (3), 46–56.

——, 1976b: Pioneer 10 and 11 observations and the dynamics of Jupiter's atmosphere. *Icarus,* **29,** 245–253.

——, and C. C. Porco, 1978: Solar heating and internal heat flow on Jupiter. *Icarus,* **35,** 27–43.

——, and Coauthors, 2004: Dynamics of Jupiter's atmosphere. *Jupiter: The Planet, Satellites, and Magnetosphere,* F. Bagenal, T. E. Dowling, and W. B. McKinnon, Eds., Cambridge University Press, 105–128.

Jeffreys, H., 1926: On the dynamics of geostrophic winds. *Quart. J. Roy. Meteor. Soc.,* **52,** 85–104.

Juckes, M. N., 2000: Linear instability of broad baroclinic zones. *Quart. J. Roy. Meteor. Soc.,* **126,** 1065–1098.

——, and M. E. McIntyre, 1987: A high resolution, one-layer model of breaking planetary waves in the stratosphere. *Nature,* **328,** 590–596.

Kida, S., 1981: Motion of an elliptic vortex in a uniform shear flow. *J. Phys. Soc. Japan,* **50,** 3517–3520.

Killworth, P. D., and M. E. McIntyre, 1985: Do Rossby-wave critical layers absorb, reflect or over-reflect? *J. Fluid Mech.,* **161,** 449–492.

Kuo, H.-L., 1951: Dynamical aspects of the general circulation and the stability of zonal flow. *Tellus,* **3,** 268–284.

Legras, B., D. G. Dritschel, and P. Caillol, 2001: The erosion of a distributed two-dimensional vortex in a background straining flow. *J. Fluid Mech.,* **441,** 369–398.

Lewis, J. M., 1998: Clarifying the dynamics of the general circulation: Phillips's 1956 experiment. *Bull. Amer. Meteor. Soc.,* **79,** 39–60.

Lighthill, M. J., 1963: Boundary layer theory. *Laminar Boundary Layers,* L. Rosenhead, Ed., Oxford University Press, 46–113.

Lorenz, E. N., 1967: *The Nature and Theory of the General Circulation of the Atmosphere.* WMO, 161 pp.

Manfroi, A. J., and W. R. Young, 1999: Slow evolution of zonal jets on the beta plane. *J. Atmos. Sci.,* **56,** 784–800.

Manney, G. L., and Coauthors, 1994: On the motion of air through the stratospheric polar vortex. *J. Atmos. Sci.,* **51,** 2973–2994.

Marcus, P. S., 1993: Jupiter's great red spot and other vortices. *Annu. Rev. Astron. Astrophys.,* **31,** 523–573.

Marshall, J., E. Shuckburgh, H. Jones, and C. Hill, 2006: Estimates and implications of surface eddy diffusivity in the Southern Ocean derived from tracer transport. *J. Phys. Oceanogr.,* **36,** 1806–1821.

McIntyre, M. E., 1970: On the non-separable baroclinic parallel flow instability problem. *J. Fluid Mech.,* **40,** 273–306. [Available online at http://www.atm.damtp.cam.ac.uk/people/mem/.]

——, 1982: How well do we understand the dynamics of stratospheric warmings? *J. Meteor. Soc. Japan,* **60,** 37–65. [Available online at http://www.atm.damtp.cam.ac.uk/people/mem/.]

——, 1994: The quasi-biennial oscillation (QBO): Some points about the terrestrial QBO and the possibility of related phenomena in the solar interior. *The Solar Engine and Its Influence on the Terrestrial Atmosphere and Climate,* E. Nesme-Ribes, Ed., NATO ASI Subseries I, Vol. 25, Springer-Verlag, 293–320.

——, and T. N. Palmer, 1983: Breaking planetary waves in the stratosphere. *Nature,* **305,** 593–600.

McWilliams, J. C., 2006: *Fundamentals of Geophysical Fluid Dynamics.* Cambridge University Press, 248 pp.

Methven, J., E. Heifetz, B. J. Hoskins, and C. H. Bishop, 2005: The counter-propagating Rossby-wave perspective on baroclinic instability. Part III: Primitive-equation disturbances on the sphere. *Quart. J. Roy. Meteor. Soc.,* **131,** 1393–1424.

Nakamura, N., 1996: Two-dimensional mixing, edge formation, and permeability diagnosed in an area coordinate. *J. Atmos. Sci.,* **53,** 1524–1537.

Niiler, P. P., and Coauthors, 2003: Near-surface dynamical structure of the Kuroshio Extension. *J. Geophys. Res.,* **108,** 3193, doi:10.1029/2002JC001461.

Norton, W. A., 1994: Breaking Rossby waves in a model stratosphere diagnosed by a vortex-following coordinate system and a technique for advecting material contours. *J. Atmos. Sci.,* **51,** 654–673.

Nozawa, T., and S. Yoden, 1997: Formation of zonal band structure in forced two-dimensional turbulence on a rotating sphere. *Phys. Fluids,* **9,** 2081–2093.

Nycander, J., D. G. Dritschel, and G. G. Sutyrin, 1993: The dynamics of long frontal waves in the shallow water equations. *Phys. Fluids,* **5,** 1089–1091.

Orr, W. M'F., 1907: The stability or instability of the steady motions of a perfect liquid and of a viscous liquid. Part I. *Proc. Roy. Irish Acad.,* **A27,** 9–68.

Pedlosky, J., 1964: The stability of currents in the atmosphere and the oceans. Part II. *J. Atmos. Sci.,* **21,** 342–353.

Phillips, N. A., 1956: The general circulation of the atmosphere: A numerical experiment. *Quart. J. Roy. Meteor. Soc.,* **82,** 123–164.

Phillips, O. M., 1972: Turbulence in a strongly stratified fluid—Is it unstable? *Deep-Sea Res.,* **19,** 79–81.

Plumb, R. A., and R. Ferrari, 2005: Transformed Eulerian-mean theory. Part I: Nongeostrophic theory for eddies on a zonal-mean flow. *J. Phys. Oceanogr.,* **35,** 165–174.

Polvani, L. M., and R. A. Plumb, 1992: Rossby wave breaking, microbreaking, fila-mentation and secondary vortex formation: The dynamics of a perturbed vortex. *J. Atmos. Sci.,* **49,** 462–476.

Reinaud, J., D. G. Dritschel, and C. R. Koudella, 2003: The shape of vortices in quasi-geostrophic turbulence. *J. Fluid Mech.,* **474,** 175–191.

Rhines, P. B., 1975: Waves and turbulence on a beta-plane. *J. Fluid Mech.,* **69,** 417–443.

——, 1977: The dynamics of unsteady currents. *The Sea,* Vol. 6, E. D. Goldberg et al., Eds., Wiley, 189–318.

——, 1994: Jets. *Chaos,* **4,** 313–339.

Riese, M., and Coauthors, 2002: Stratospheric transport by planetary wave mixing as observed during CRISTA-2. *J. Geophys. Res.,* **107,** 8179, doi:10.1029/2001JD000629.

Robinson, W. A., 1988: Analysis of LIMS data by potential vorticity inversion. *J. Atmos. Sci.,* **45,** 2319–2342.

——, 2006: On the self-maintenance of midlatitude jets. *J. Atmos. Sci.,* **63,** 2109–2122.

Rogers, J. H., 1995: *The Giant Planet Jupiter.* Cambridge University Press, 418 pp.

Rosenlof, K. H., 1995: Seasonal cycle of the residual mean meridional circulation in the stratosphere. *J. Geophys. Res.,* **100,** 5173–5191.

Ruddick, B. R., T. J. McDougall, and J. S. Turner, 1989: The formation of layers in a uniformly stirred density gradient. *Deep-Sea Res.,* **36,** 597–609.

Salmon, R., 1982: Geostrophic turbulence. *Topics in Ocean Physics,* A. Osborn and P. Malanotte-Rizzoli, Eds., North-Holland, 30–78.

Scott, R. K., and L. M. Polvani, 2007: Forced-dissipative shallow water turbulence on the sphere and the atmospheric circulation of the giant planets. *J. Atmos. Sci.*, **64,** 3158–3176.

Simmons, A. J., 1974: The meridional scale of baroclinic waves. *J. Atmos. Sci.,* **31,** 1515–1525.

——, M. Hortal, G. Kelly, A. McNally, A. Untch, and S. Uppala, 2005: ECMWF analyses and forecasts of stratospheric winter polar vortex break-up: September 2002 in the Southern Hemisphere and related events. *J. Atmos. Sci.,* **62,** 668–689.

Sommeria, J., S. D. Meyers, and H. L. Swinney, 1989: Laboratory model of a planetary eastward jet. *Nature,* **337,** 58–61.

——, ——, and ——, 1991: Experiments on vortices and Rossby waves in eastward and westward jets. *Nonlinear Topics in Ocean Physics,* A. R. Osborne, Ed., North-Holland, 227–269.

Starr, V. P., 1968: *Physics of Negative Viscosity Phenomena.* McGraw-Hill, 256 pp.

Stewartson, K., 1978: The evolution of the critical layer of a Rossby wave. *Geophys. Astrophys. Fluid Dyn.,* **9,** 185–200.

Stone, P. H., 1969: The meridional structure of baroclinic waves. *J. Atmos. Sci.,* **26,** 376–389.

——, 1976: The meteorology of the Jovian atmosphere. *Jupiter,* T. Gehrels, Ed., University of Arizona Press, 586–618.

Sukoriansky, S., N. Dikovskaya, and B. Galperin, 2007: On the "arrest" of inverse energy cascade and the Rhines scale. *J. Atmos. Sci.*, **64,** 3312–3327.

Taylor, G. I., 1915: Eddy motion in the atmosphere. *Philos. Trans. Roy. Soc. London,* **A215,** 1–23.

Theiss, J., 2004: Equatorward energy cascade, critical latitude, and the predominance of cyclonic vortices in geostrophic turbulence. *J. Phys. Oceanogr.,* **34,** 1663–1678.

Thompson, A. F., and W. R. Young, 2007: Two-layer baroclinic eddy heat fluxes: Zonal flows and energy balance. *J. Atmos. Sci.,* **64,** 3214–3231.

Thompson, R. O. R. Y., 1971: Why there is an intense eastward current in the North Atlantic but not in the South Atlantic. *J. Phys. Oceanogr.,* **1,** 235–237.

Thomson, W. (Lord Kelvin), 1887: Stability of fluid motion—

Rectilineal motion of viscous fluid between two parallel planes. *Philos. Mag.,* **24,** 188–196.

Thorncroft, C. D., and Coauthors, 1993: Two paradigms of baroclinic-wave life-cycle behaviour. *Quart. J. Roy. Meteor. Soc.,* **119,** 17–55.

Vallis, G. K., and M. E. Maltrud, 1993: Generation of mean flows and jets on a beta plane and over topography. *J. Phys. Oceanogr.,* **23,** 1346–1362.

Viúdez, A., and D. G. Dritschel, 2004: Optimal potential vorticity balance of geophysical flows. *J. Fluid Mech.,* **521,** 343–352.

Warn, T., and H. Warn, 1978: The evolution of a nonlinear critical level. *Stud. Appl. Math.,* **59,** 37–71.

Waugh, D. W., and D. G. Dritschel, 1991: The stability of filamentary vorticity in two-dimensional geophysical vortex-dynamics models. *J. Fluid Mech.,* **231,** 575–598.

——, and Coauthors, 1994: Transport of material out of the stratospheric Arctic vortex by Rossby wave breaking. *J. Geophys. Res.,* **99,** 1071–1078.

Whitehead, J. A., 1975: Mean flow generated by circulation on a beta-plane: An analogy with the moving flame experiment. *Tellus,* **27,** 358–363.

Williams, G. P., 2003: Jovian dynamics. Part III: Multiple, migrating, and equatorial jets. *J. Atmos. Sci.,* **60,** 1270–1296.

Yamagata, T., 1976: On trajectories of Rossby-wave packets released in a lateral shear flow. *J. Oceanogr. Soc. Japan,* **32,** 162–168.